Energy 44 (2012) 358–366

Contents lists available at SciVerse ScienceDirect

Energy

journal homepage: www.elsevier.com/locate/energy

Hydrate-based CO_2 (carbon dioxide) capture from IGCC (integrated gasification combined cycle) synthesis gas using bubble method with a set of visual equipment

Chun-Gang Xu [a,b], Xiao-Sen Li [a,b,*], Qiu-Nan Lv [a,b], Zhao-Yang Chen [a,b], Jing Cai [a,b]

[a] Key Laboratory of Renewable Energy and Gas Hydrate, Guangzhou Institute of Energy Conversion, Chinese Academy of Sciences, Guangzhou 510640, PR China
[b] Guangzhou Center for Gas Hydrate Research, Chinese Academy of Sciences, Guangzhou 510640, PR China

ARTICLE INFO

Article history:
Received 3 February 2012
Received in revised form
7 May 2012
Accepted 7 June 2012
Available online 6 July 2012

Keywords:
Hydrate
CO_2 separation
Bubble
Visual equipment
Gas consumed
IGCC

ABSTRACT

The hydrate-based carbon dioxide (CO_2) capture from the integrated gasification combined cycle (IGCC) synthesis gas using the bubble method is investigated with a set of visual equipment in this work. The gas bubble is created with a bubble plate on the bottom of the equipment. By the visual equipment, the hydrate formation and the hydrate shape are visually captured. With the move of the gas bubble from the bottom to the top of the reactor, gas hydrate forms firstly from the gas–liquid boundary around the bubble, then the hydrate gradually grows up and piles up in the bottom side of the bubble to form a hydrate particle. The gas hydrate shape is affected by the gas flow rate. The hydrate is acicular crystal at the low gas flow rate while the hydrate is fine sand-like crystal at the high gas flow rate. The bubble size and the gas flow rate have an obvious impact on the hydrate-based CO_2 separation process. The experimental results show the gas bubble of 50 μm and the gas flow rate of 6.75 mL/min/L are ideal for CO_2 capture from IGCC synthesis gas under the condition of 3.0 MPa and 274.15 K.

1. Introduction

Carbon dioxide (CO_2) is considered as the main contributor to the greenhouse gases which result in the global warming, and the fuel power plants produce nearly one third of all CO_2 emissions worldwide [1,2]. Therefore, capturing CO_2 from fossil power plants becomes one urgent target for lessening the deteriorating climate. Recently, the integrated gasification combined cycle (IGCC) is widely utilized in coal-fired power plants. Thus, capturing CO_2 and purifying hydrogen (H_2) from IGCC synthesis gas becomes one important project for the industrial application. The typical synthesis gas from an IGCC power station consists of 40 mol% CO_2 and 60 mol% hydrogen (H_2) at a total pressure of 2.5–5.0 MPa [3]. Conventional techniques for the CO_2 capture include physical adsorption, chemical absorption, cryogenic fractionation, and membrane separation [4,5]. However, the conventional techniques have their individual issues of either high corrosion, or large energy consumption, or high cost, or low capacity [6]. Therefore, for using fossil fuels in the power plants continuously, new efficient and more cost-effective techniques which are different from the conventional techniques need to be explored. One of such technique is hydrate-based technique of gas separation and capture. Gas hydrate is one crystalline compound formed by host (water molecules) and guest (small gas molecules such as methane (CH_4), ethane (C_2H_6), propane (C_3H_8), sulfurated hydrogen (H_2S), CO_2, H_2, nitrogen (N_2)) [7,8]. The hydrate-based technique of gas separation is on the selective partition of the ingredients in the hydrate phase and in the gas phase [1]. Due to the equilibrium hydrate formation pressure of CO_2 is much lower than that of H_2 at the same temperature, it is expected that CO_2 is preferentially encaged into the hydrate crystals. Then, the hydrate crystals are separated and subsequently decomposed to create the CO_2-rich stream while the rest form the CO_2-lean one [9,10].

However, there are two important problems need to be resolved for hydrate-based gas separation technology. One is to form the hydrate rapidly and continually, the other is to improve the gas uptake dramatically. Some methods have been proposed to increase the hydrate formation. The methods are mainly classified two: chemical and mechanical methods. In the chemical aspect, the hydrate formation rate can be increased efficiently by adding either the thermodynamic promoters (for example, tetrahydrofuran (THF)

* Corresponding author. Key Laboratory of Renewable Energy and Gas Hydrate, Guangzhou Institute of Energy Conversion, Chinese Academy of Sciences, Guangzhou 510640, PR China. Tel.: +86 20 87057037; fax: +86 20 87034664.
E-mail addresses: xucg@ms.giec.ac.cn (C.-G. Xu), lixs@ms.giec.ac.cn (X.-S. Li).

0360-5442/$ – see front matter © 2012 Elsevier Ltd. All rights reserved.
http://dx.doi.org/10.1016/j.energy.2012.06.021

[11,12] or tetra-n-butyl ammonium bromide (TBAB) [6,10]) or kinetics promoters (for example, sodium dodecyl sulfate (SDS) [13,14]). For example, the TBAB solution of 0.29 mol% is proved to be efficient to decrease the equilibrium hydrate formation pressure and to improve the gas uptake for CO_2 separation from fuel gases [15,16]. In the mechanical aspect, the hydrate formation can be enhanced by stirring [17–19], spraying [20,21], and bubbling [22]. The different mechanical methods match to the different hydrate reactors, such as a stirred tank, spray tower and the bubble tower. Among the three mechanical methods, the stirring is usually used to carry out the hydrate formation because the stirred tank is easy to build and run on a laboratory scale. Several works have been reported on the hydrate formation in a batch stirred tank [18,23]. However, the stirred tank is not easy to be thoroughly sealed in a high-pressure condition. Moreover, the stirred tank and the sprayer tank consume much energy when they work. The gas bubble is created by pouring the gas mixture from the gas tank into the solution in the reactor. Thus, the method of bubbling consumes little energy. Some works on hydrate formation in bubble columns have been published [24–27]. Nevertheless, up to now, no systematical work on hydrate formation in a bubble column has been reported on the hydrate-based CO_2 capture from IGCC synthesis gases. Therefore, we make a series of experiments to study on hydrate-based CO_2 capture from IGCC synthesis gas in a bubble column systematically.

In this work, a set of transparent bubble column is established and the CO_2 separation from IGCC synthesis gas in the presence of 0.29 mol% TBAB solution is studied. (0.29 mol% TBAB is proved to be the ideal hydrate formation promoter in our previous work [6,10]). Meanwhile, according to the previous work [6,10], the hydrate formation condition of 3.0 MPa and 274.15 K is proved to be a good condition for CO_2 capture from IGCC synthesis gas with the TBAB solution. Thus, the condition is adopted in this work. The work is carried out as follows: firstly, the formation of the hydrate containing TBAB, gas mixture and H_2O and the detailed shape of the hydrate are captured by the transparent column; secondly, by the comparison of hydrate formation induction time, CO_2 separation efficiency obtained from our previous experiments and this work, the equipment of a transparent bubble column is proved to be available to the hydrate-based CO_2 capture from IGCC synthesis gas; thirdly, by the comparisons of the gas uptake, the CO_2 concentration in the residual gas obtained from different bubble sizes and the gas flow rates, an ideal hydrate-based CO_2 separation in a bubble column is proposed and the results are helpful to develop and design an industrial hydration reactor in the future.

2. Experimental section

2.1. Materials

A CO_2/H_2 gas mixture with a molar ratio of 40.0–60.0% is used in the work to simulate a pretreated IGCC synthesis gas. The gas mixture is supplied by Foshan Huate Gas Co., Ltd. TBAB (AR, >99.9%) is supplied by Shanghai Sinopharm Chemical Reagent Co., Ltd., China. The deionized water with resistivity of 18.25 mΩ cm^{-1} is produced by an ultrapure water supplied by Nanjing Ultrapure Water Technology Co., Ltd., China.

2.2. Apparatus

The experimental apparatus are shown in Fig. 1. It consists of a cuboid reactor (10.0 cm in side length, 4.0 m in height, total volume of 40 L) made of 316 stainless steel and a refrigeration,

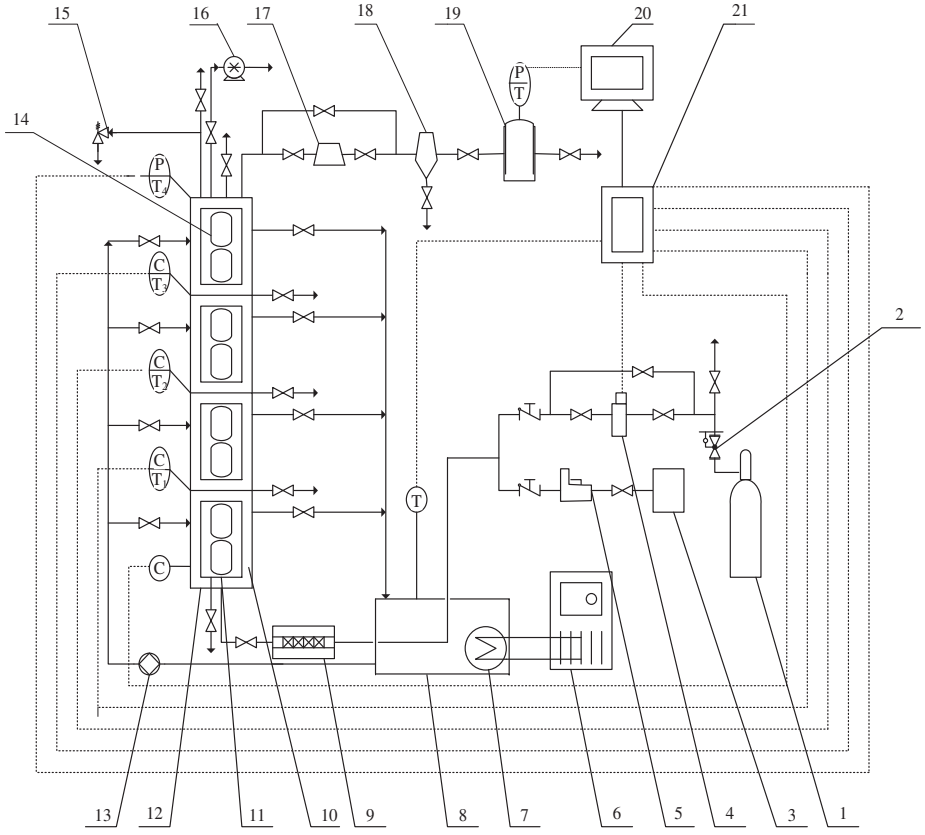

Fig. 1. Schematic of experimental apparatuses. (1. Gas cylinder 2. Relief valve 3. Fluid container 4. Mass flow-meter 5. Controlled volume pump 6. Refrigeration system 7. Heater exchanger 8. Coolant tank 9. Static mixer 10. Water bath 11. Distributor 12. Reactor 13. Coolant recycle pump 14. Visual window 15. Safety valve 16. Vacuum pump 17. PID pressure controller 18. Gas-liquid separator 19. Collecting gas cylinder 20. PC 21. Data acquisition system).

a temperature control unit and two pumps. The reactor is equipped with transparent Plexiglas in front and back sides and is jacketed with the glycol-water bath with right and left sides. The reactor is evenly divided into four parts from bottom to top (part I, II, III, IV). The maximum working pressure for the reactor is 4.0 MPa. A scalar with a precision of 1 cm attached to a side of the reactor is used to mark the detailed position. The range of the scalar is 0–400 cm. The temperature range of the glycol-water bath can be regulated from −5 °C to 40 °C with an accuracy of ±0.2 °C. The temperature in the reactor is controlled by the glycol-water flowing circularly in the jacket out of the reactor. A Pt1000 thermoprobe with an accuracy of ±0.05 °C is settled on the top of each part to measure the temperature. The pressure in the experimental apparatuses is measured using a pressure transducer, with range of (0–10) MPa and an accuracy of ±0.02 MPa. The pressure in the reactor is controlled by a proportional-integral-derivative (PID) controlled pressure regulated valve (Tescom ER3000) with a pressure-controlling accuracy of ±0.02 MPa. A gas flow-meter (LineTech M3030) determines the gas volume introduced from the gas cylinder. The flow rate range for the flow-meter is (0–22.5 mL/min/L). Due to the whole volume of the cuboid reactor is fixed at 40 L, the unit of volume per min per reactor volume is adopted as the unit of the gas flow rate in this work. The bubble size is controlled by a round bubble plate (10 cm in diameter). The bubble plate is installed at the bottom of the cuboid for creating bubbles. In the work, the bubble plates of 20 μm, 50 μm, 100 μm are used. Fig. 2 shows the picture of the real visual reactor in the experiment. As shown in Fig. 2, four parts can be seen clearly.

Fig. 2. Picture of the visual reactor.

2.3. Procedure

Each experimental run is performed according to the following sequence of steps:

1 the equipment is washed with distilled water and evacuated. Then, the 0.29 mol% TBAB solution with desired volume of 36 L is pumped into the reactor using a vacuum pump. Subsequently, the reactor is flushed with the CO_2/H_2 gas mixture at least four times to remove any residual air or mixed gas.
2 set the temperature T at a desired value, then, turn on the refrigeration and glycol-water bath recycle pump.
3 after the temperature T has stabilized at the preset value for more than 2 h, CO_2/H_2 gas mixture is introduced into the reactor via a gas flow-meter at a flow rate. When the pressure in the reactor exceeds 3.05 MPa, the PID starts to release the gas to the collecting gas cylinder (CGC) to keep the pressure constant at approximately 3.0 MPa.
4 the motion of the bubbles in the reactor and the hydrate formation are captured by a Sony camera (HDR-XR100E). The data on temperature, pressure and the gas mixture are collected by an automatic data acquisition system (Agilent 34970A) connected with a computer.
5 after the hydrate formation completion (there is no hydrate formation and the pressure in the CGC rises linearly for more than 1-h), the residual gas is collected with a sampling gaseous envelope. Then, the residual gas is analyzed using a gas chromatograph (GC) (HP6890).
6 finally, the reactor is quickly depressurized to atmospheric pressure. Then, the refrigeration system is shut off, and the heating system is started. After the temperature in the reactor reaches 18 °C and the temperature is kept for more than 1-h, subsequently, the gas evolved from the decomposed hydrate and released from the solution is collected and analyzed by GC.

3. Result and discussion

3.1. Hydrate formation and shape

Fig. 3(a) describes the hydrate formation in the process of the gas bubble moving from bottom to top for gas bubble size of 50 μm and gas flow rate of 6.75 mL/min/L at 3.0 MPa and 274.15 K. In the Fig. 3(a), eight sectional drawings intercepted in 1 s intervals from an 8 s video of the whole hydrate formation are orderly listed. As shown in Fig. 3(a), the hydrate forms firstly from the gas–liquid boundary around the bubble, then, the hydrate gradually grows up and piles up in the bottom side of the bubble to form a gas hydrate particle. The gas hydrate particle consists of a gas bubble and hydrates. In the gas hydrate particle, the gas bubble looks like a head in the top of the hydrate particle and the hydrate looks like a tail adhering tightly the gas bubble. The bubble shrinks because CO_2 is being formed into the hydrate to form hydrate particle continuously. In the process, when the buoyancy resulted from the gas bubble is greater than the gravity of the gas hydrate particle in the solution, the gas hydrate particle moves up along the reactor, otherwise, the gas hydrate particle goes down and piles up in the bottom of the reactor because the specific gravity of TBAB gas hydrate is greater than the TBAB solution. As seen from Fig. 3(a), for example, a small gas hydrate particle with a small gas bubble on the top is captured clearly in its process of rising in the reactor, and its detailed position pointed with a red arrow in the same reactor is individually shown in Pictures 1–6. A big gas hydrate particle which has the same moving is also pointed with purple

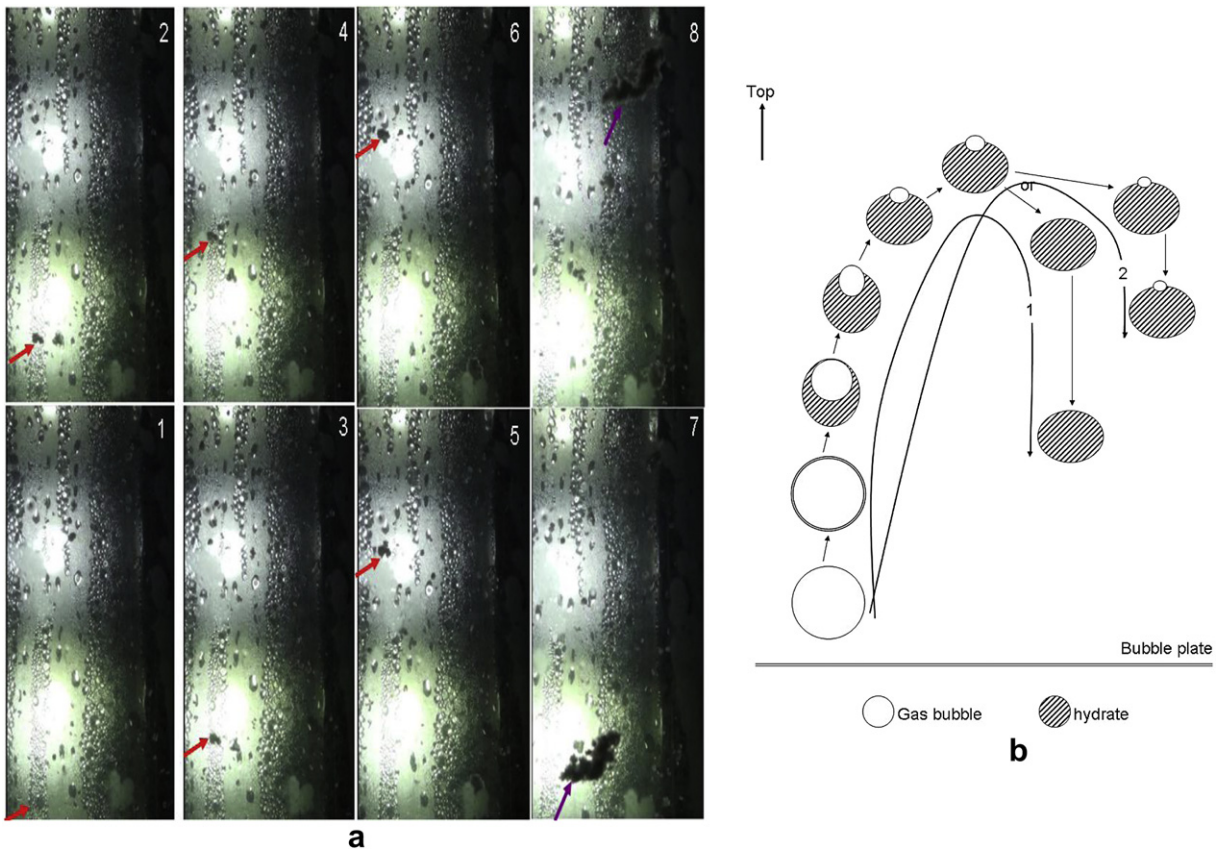

Fig. 3. (a) Hydrate formation process in the process of the gas bubble moving from bottom to top for the gas bubble of 50 μm and at the gas flow rate of 6.75 mL/min/L at 3.0 MPa and 274.15 K. (b) Schematic line drawing of hydrate formation process in the process of the gas bubble moving from bottom to top.

arrows in Pictures 7 and 8. The different positions shown in the pictures 1–8 reflect the continuous moving of the hydrate particle in the reactor. Besides, some small hydrate particles without any gas bubbles or with quite small gas bubbles dropping down are also captured in the Fig. 3(a). In order to clearly interpret the hydrate formation process, a schematic line drawing of hydrate formation process in the process of the gas bubble moving from bottom to top is made, as seen in Fig. 3(b). As seen in Fig. 3(b), the gas bubble is created by a bubble plate and it moves up in the TBAB solution because of buoyancy. Then, a thin gas–liquid interface is formed in the outer surface of the bubble and gas hydrate start to form in the interface. Then, the gas bubble shrinks because CO_2 is encaged in the hydrate gradually. Meanwhile, the hydrate grows up and aggregates. Next, some gas bubbles suddenly break and the hydrates start to drop because of their gravity, and finally the hydrates pile up on the wall of the reactor, and this is depicted as route 1 in Fig. 3(b). Some other gas bubbles do not break. Then, the gas hydrate particles start to drop and pile up on the wall of the reactor after the gravity of the hydrates is bigger than the buoyancy of the gas bubbles in the solution, and this is depicted as route 2 in Fig. 3(b).

In the process of the gas bubbles moving from bottom to top, most of the small gas bubbles lessen because they are transformed to the gas hydrates. However, not all the gas bubbles are transformed to the gas hydrate particles. As seen from Fig. 3(a), the big bubbles of diameters more than 2.2 mm do not be transformed to the gas hydrate particles. After they move to the top of the solution, some collapse and some gather in the lower surface of the gas–liquid solution boundary because of surface tensions. At the boundary, the gas hydrates easily form because the more gases exist at the top of the boundary. Thus, those bubbles gathering in the lower surface of the gas–liquid solution boundary shrink due to the CO_2 molecules entrap into the hydrates. After then, the hydrate particles transformed from the bubbles drop down because of the gravity. Fig. 4 describes the hydrate formation in the gas-solution boundary for the gas bubble of 50 μm and at the gas flow rate of 6.75 mL/min/L at 3.0 MPa and 274.15 K. As shown in Fig. 4, a piece of hydrate (pointed with a long red arrow) drops down from the lower surface after the gases involving in the piece of the hydrate-gas bubble particle entrap into the hydrates. Pictures a ∼ d are captured every 2 s. As seen from pictures a–d in Fig. 4, the drop process of the piece of hydrate is observed clearly, and the detailed positions of the hydrate particle in pictures a–d are marked with red arrows on an enlarged measuring scalar. Then, the hydrate particle starts to drop from the height of 360 cm (as shown in picture a), and 6 s later, the particle drops to the height of approximately 358 cm (as shown in picture d).

Fig. 5 shows the hydrate shape in the reactor for gas bubble of 50 μm and at the gas flow rate of 6.75 mL/min/L at 3.0 MPa and 274.15 K. After the hydrate formation completion, as shown in Fig. 5, most of the hydrates pile up at the bottom of the reactor, part of the hydrates pile up on the wall of the reactor because the temperature in the wall of the reactor is the lowest and the heat transfer in the site is quite rapid. The phenomenon further proves the theory of the hydrate growth along the wall [28,29]. The gas hydrate looks like acicular crystal. However, the gas hydrate shape is affected by the gas flow rate. With the gas flow rate increase, the acicular crystal of the gas hydrate gradually changes to the shape like fine sand. Fig. 6 shows the gas hydrate shape for gas bubble of 50 μm and at the gas flow rate of 22.5 mL/min/L at 3.0 MPa and 274.15 K. As seen from Fig. 6, no acicular crystal can be found in the reactor while the reactor is filled with those hydrates look like fine sands. The reason might be that the acicular structure is destroyed by the vigorous turbulence resulted from the high gas flow rate.

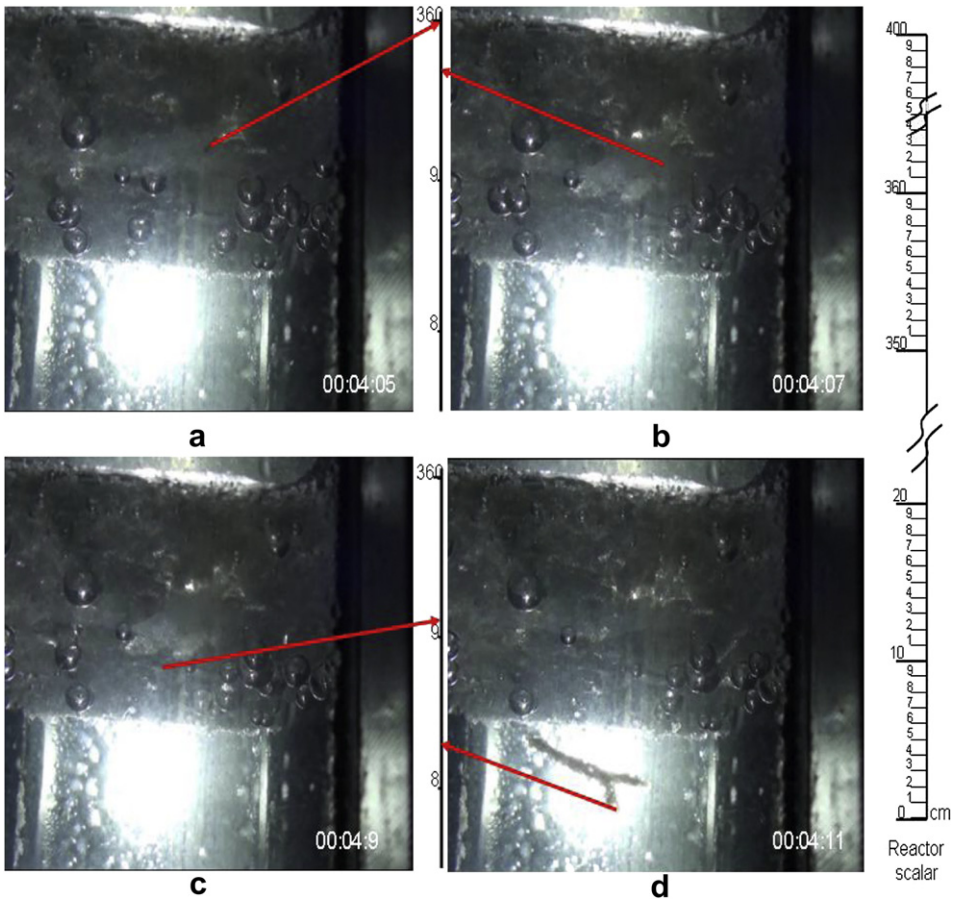

Fig. 4. Hydrate formation process in the gas-solution boundary for the gas bubble of 50 μm and at the gas flow rate of 6.75 mL/min/L at 3.0 MPa and 274.15 K. (note: the reactor scalar schema is showed in the right of the figure, the whole height of the reactor is 400 cm. The hydrate particle positions are marked on an amplified scalar in the figure with red arrows). (For interpretation of the references to color in this figure legend,the reader referred to the web version of this article.)

Fig. 7 shows one clip of the hydrate dissociation in 3 s. As shown in Fig. 7, many gases rapidly release from the gas hydrate slurries once the depressurization is started. The enormous gases agitate the system vigorously and the agitation results in the hydrates spreading in the whole reactor quickly. Meanwhile, more gases are released from the hydrates. The phenomenon proves the enormous gases are encaged in the hydrates.

3.2. Effect of bubble size

Table 1 shows the comparison of the CO_2 concentrations in the residual gases at different experimental conditions. As shown in Table 1, compared to our previous work, the CO_2 concentrations in the residual gases in the system are close to the results obtained from the small experimental systems [15]. For example, the CO_2 concentrations in residual gases at the small experimental systems are from 15.1 mol% to 21.3 mol% while those at this visual system are from 13.6 mol% to 23.7 mol%. That means, although the volume of the reactor is approximately 100 times larger than the small reactor (volume of 400 mL in our previous experiments) and the bubble system for mixing gas–liquid in the experiment replaces the stirring system in our previous experiments, the experimental results obtained in this work are similar to those obtained in the previous experiments and the visual equipment is proved to be reliable to the hydrate-based CO_2 capture from IGCC synthesis gases.

Fig. 8 shows the change of gas consumed and CO_2 concentration in the residual gases with bubble sizes at the gas flow rate of 6.75 mL/min/L at 3.0 MPa and 274.15 K. As shown in Fig. 8, among the three bubbles of (20 μm, 50 μm and 100 μm), the highest gas consumed and the lowest CO_2 concentration in the residual gas phase are obtained when the bubble size is fixed at 50 μm. For example, the gas consumed for the gas bubble of 50 μm is 411.0 L, while those for the gas bubbles of 20 μm and 100 μm are 143.8 L and 190.0 L, respectively. It means the gas bubble size has an obvious effect on the hydrate-based CO_2 capture from the IGCC synthesis gas. Either too big or too small size of the gas bubble is not helpful to the gas consumed in the hydrate-based process. The bigger size of the gas bubble results in the smaller gas–liquid boundary, and it further results in the smaller gas entrapping into the hydrate to form gas hydrate. However, although the smaller size of the gas bubble provides the bigger gas–liquid boundary, the smaller bubble causes little turbulence when it moves from the bottom to the top. In fact, the gas bubble of 20 μm does move uprightly when the gas bubble moving rate is controlled at approximately 6.75 mL/min/L. However, the gas bubbles of 50 μm and 100 μm move to the top with the obvious sway at the same rate. The sway causes the enough convection of the solution around the gas bubbles. Thus the convection further results in the faster heat-exchange between the gas and the solution, and it finally promotes the gas hydrate formation.

The CO_2 concentration in the residual gas phase reflects the selectivity of CO_2 in the hydrate-based process. Due to the volume of the residual gas phase is fixed, the lower CO_2 concentration in the residual gas phase means the more CO_2 is encaged into the gas hydrate selectively when the amount of the gas consumed obtained from different experiments are same. It does also mean the process

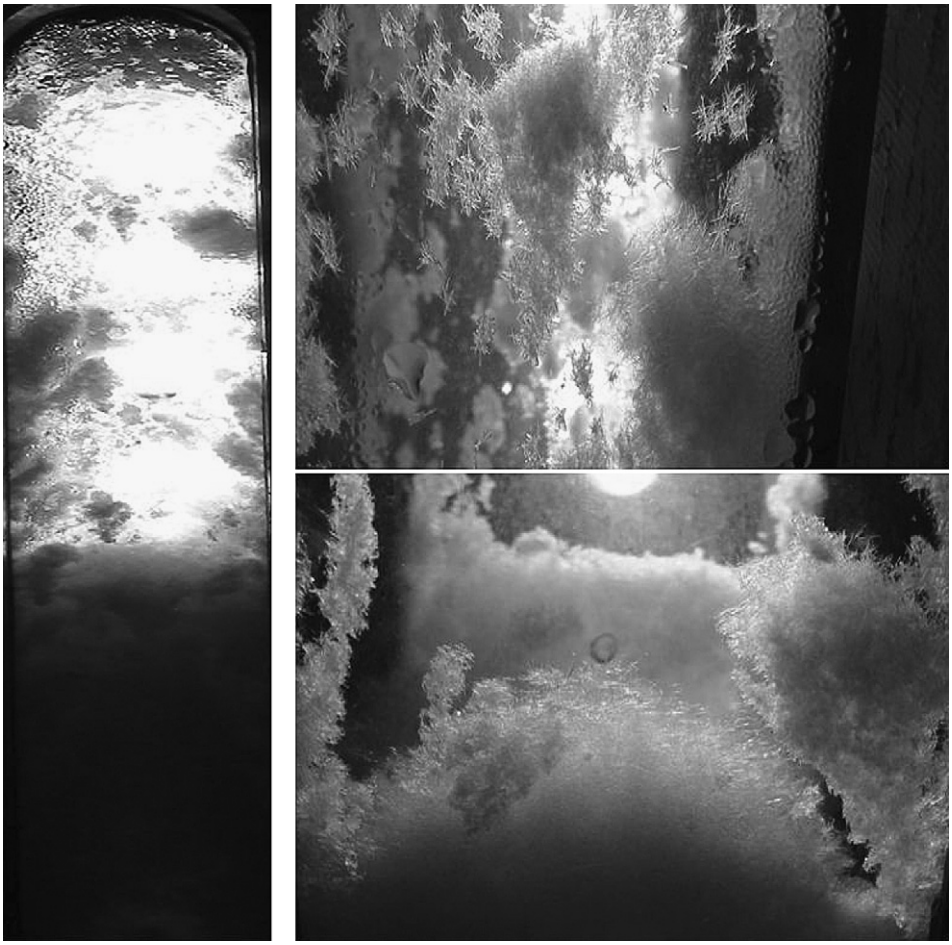

Fig. 5. Hydrate shape in the reactor for the gas bubble of 50 μm and at the gas flow rate of 6.75 mL/min/L at 3.0 MPa and 274.15 K.

Fig. 6. Gas hydrate shape for the gas bubble of 50 μm and at the gas flow rate of 22.5 mL/min/L at 3.0 MPa and 274.15 K.

Fig. 7. Hydrate dissociation process.

which is adopted to obtain the lower CO_2 concentration in the residual gas phase is more efficient to capture CO_2 from IGCC synthesis gases. Corresponding with the relationship of the gas consumed vs. the bubble size, the CO_2 concentration in the residual gas phase obtained from the process for the gas bubble of 50 μm is 13.6 mol% which is lower than 23.7 mol% and 18.85 mol% obtained from the processes for the gas bubbles of 20 μm and 100 μm, respectively. In other words, the result reflected from the CO_2 concentration curve in Fig. 8 further proves that the bubble size has an obvious effect on the gas hydrate formation and the bubble of 50 μm is the best among the three bubble sizes (20 μm, 50 μm and 100 μm) for hydrate-based CO_2 capture from IGCC synthesis gas.

Table 1
Comparison of CO_2 concentration in residual gas after hydrate formation completion at different experimental conditions.

Experimental conditions	CO_2 concentration in residual gases
0.29 mol% TBAB at 277.05 K and 2.72 MPa [15]	18.5 mol%
0.29 mol% TBAB at 278.15 K and 3.0 MPa [15]	21.3 mol%
0.29 mol% TBAB + 5 vol% CP at 274.15 K and 4.0 MPa [10]	15.1 mol%
Bubble size of 100 μm + 0.29 mol% TBAB at 274.15 K and 3.0 MPa in this work	18.9 mol%
Bubble size of 50 μm + 0.29 mol% TBAB at 274.15 K and 3.0 MPa in this work	13.6 mol%
Bubble size of 20 μm + 0.29 mol% TBAB at 274.15 K and 3.0 MPa in this work	23.7 mol%

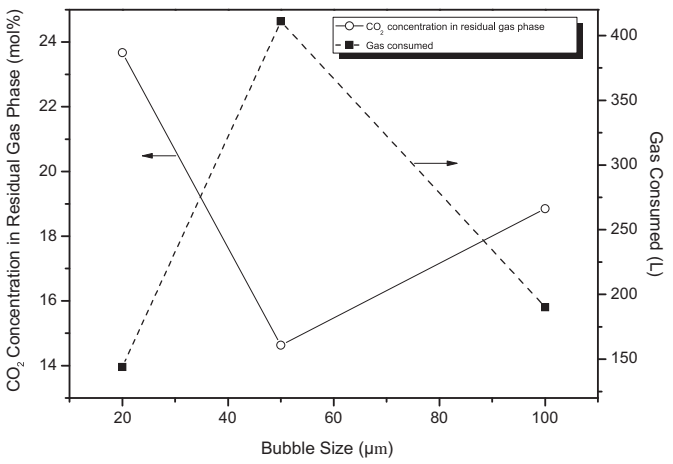

Fig. 8. CO_2 concentration in residual gas phase and the gas consumed change vs. the gas bubble size at the gas flow rate of 6.75 mL/min/L at 3.0 MPa and 274.15 K.

Fig. 9 shows the pressure in the reactor changes with time in the processes for the three bubble sizes (20 μm, 50 μm and 100 μm) at 274.15 K. As shown in Fig. 9, the time for the pressure in the reactor reaching 3.0 MPa, (i.e., the time of hydrate formation completion), for the three bubble sizes (20 μm, 50 μm and 100 μm) are 8.87 h, 11.72 h and 10.33 h, respectively, at the gas flow rate of 6.75 mL/min/L. The slope of the curve from 0 to 3.0 MPa shows the rising rate of the pressure, and it also reflects the rate of gas mixture consumption. In other words, the smaller slope of the curve implies the bigger rate of the gas consumption. As shown in Fig. 9, the slopes of the curves for the three bubble sizes are summarized as 20 μm > 100 μm > 50 μm. Therefore, the gas consumption rate for the gas bubble of 50 μm is the highest. Besides, as shown in Fig. 9, the pressure in the reactor keeps constant at approximately 3.0 MPa for some time. In this time, the gas consumed resulting from the hydrate formation almost equals to the gas supplied into the reactor. When the gas consumed rate decreases, the pressure in the reactor increases observably. When the pressure is bigger than 3.05 MPa, the PID starts to release gas and to keep the pressure in the reactor at approximately 3.0 MPa. Fig. 9 shows that the term (pressure is kept at approximately 3.0 MPa) for the gas bubble of 50 μm are 9.96 h, and it is far longer than those for the gas bubbles of 20 μm and 100 μm, respectively. It means the gas consumption in this term for the gas bubble of 50 μm is large while those for the gas bubbles of 20 μm and 100 μm are small. It further illustrates that compared to the gas bubbles of 20 μm and 100 μm, the gas bubble of 50 μm is quite favorable to the process of hydrate-based CO_2 capture from IGCC synthesis gases.

3.3. Effect of gas flow rate

Fig. 10 shows the CO_2 concentration in the residual gas phase and the gas consumed for the gas bubble of 50 μm under different gas flow rates (4.50 mL/min/L, 5.63 mL/min/L, 6.75 mL/min/L, 11.25 mL/min/L, 15.75 mL/min/L, 22.50 mL/min/L) at 274.15 K. As shown in Fig. 10, when the gas flow rate is lower than 6.75 mL/min/L, either CO_2 concentration in the residual gas phase and the gas consumed has little change. However, when the gas flow rate is higher than 6.75 mL/min/L, the increase of the gas flow rate results in the increase of the CO_2 concentration and the decrease of the gas consumed. For example, the CO_2 concentrations are 8.9 mol%, 9.1 mol% and 8.9 mol% for the gas flow rate of 4.50 mL/min/L, 5.63 mL/min/L and 6.75 mL/min/L, respectively, and they are obviously lower than 13.5 mol%, 13.6 mol%, 13.8 mol% for gas flow rates of 11.25 mL/min/L, 15.75 mL/min/L and 22.50 mL/min/L, respectively. Besides, the gas consumed for the gas flow rate of 4.50 mL/min/L, 5.63 mL/min/L and 6.75 mL/min/L are 410.0 L, 396.5 L and 411.0 L, respectively, which are at least 15% higher than those for other gas flow rates. It illustrates when the change of the gas flow rate has little effect on the CO_2 separation when the gas flow rate is lower than 6.75 mL/min/L, nevertheless, it has an adverse impact on the CO_2 separation when the gas flow rate is higher than 6.75 mL/min/L. Thus, it means the gas flow rate of 6.75 mL/min/L is optimal in this work.

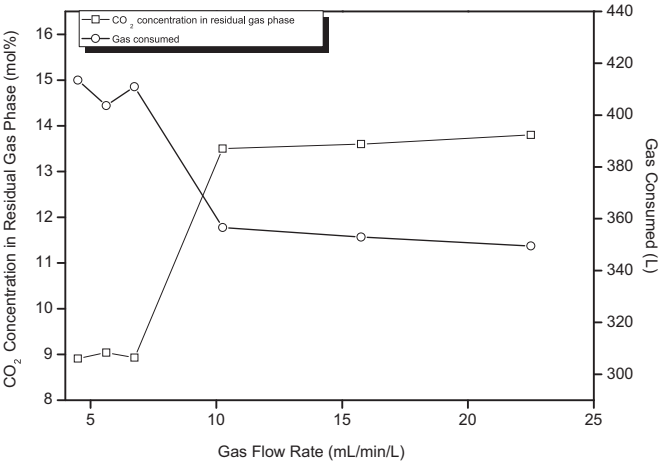

Fig. 10. CO_2 concentration in residual gas phase and gas consumed change with gas flow rate for the gas bubbles of 50 μm at 3.0 MPa and 274.15 K.

Fig. 11 shows pressure in CGC changes with the gas flow rate at 274.15 K. The pressure in the CGC is resulted from the gas released from the reactor under the driving of PID when the pressure in the reactor is more than 3.05 MPa. The higher pressure in the CGC means the more gas introduced from the gas cylinder is not be effectively separated in the process. As shown in Fig. 11, when the gas flow rate changes from 4.50 mL/min/L to 6.75 mL/min/L, the pressure in CGC has little change. However, the pressure in the CGC increases with the increase of the gas flow rate when the gas flow

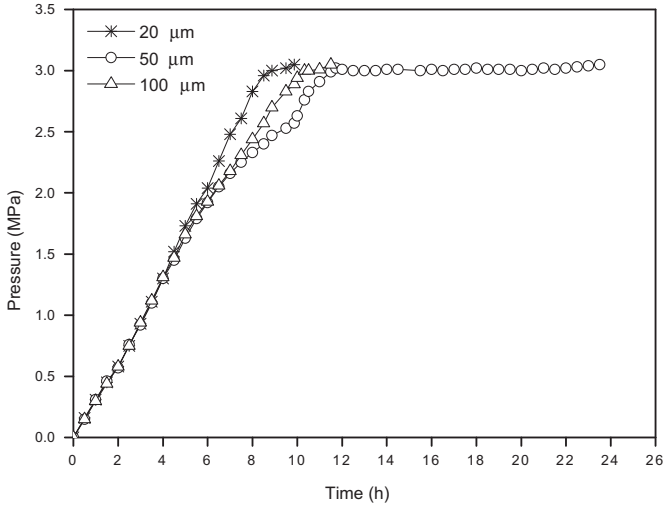

Fig. 9. Pressures in the reactor change with time for the gas bubbles of (20 μm, 50 μm and 100 μm) at the gas flow rate of 6.75 mL/min/L at 3.0 MPa and 274.15 K.

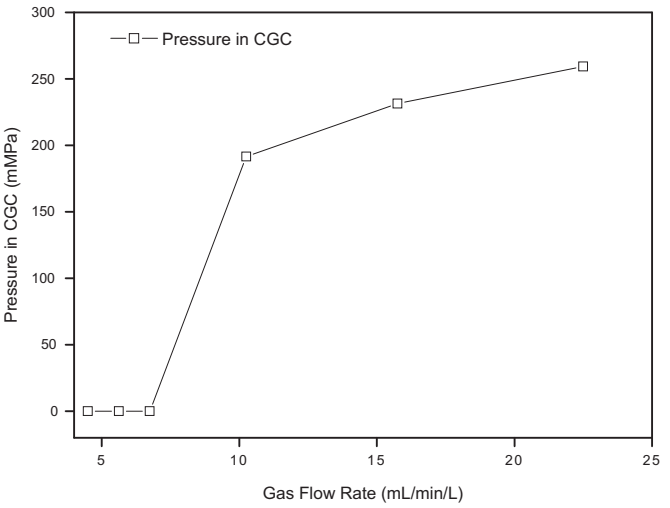

Fig. 11. Pressure in CGC changes with gas flow rate for the gas bubble of 50 μm at 3.0 MPa and 274.15 K.

rate is higher than 6.75 mL/min/L, and this phenomenon can be attributed to that the hydrate formation rate is lower than the gas flow rate. Therefore, it is necessary to find one balance between the two rates. Seen from Fig. 11, the pressure in the CGC is zero when the gas flow rate is not bigger than 6.75 mL/min/L, that is, no any gas is released into the CGC at the rate, and it indicates that there is one balance between the hydrate formation rate and the gas flow rate of 6.75 mL/min/L.

4. Conclusion

Hydrate-based carbon dioxide (CO_2) capture from the integrated gasification combined cycle (IGCC) synthesis gas using the bubble method is investigated with a set of visual equipment in this work. The gas bubble is created with a bubble plate on the bottom of the equipment. By the visual equipment, the hydrate formation process and the hydrate shape are visually captured. In the process of the gas bubble moving from the bottom to the top of the reactor, the gas hydrate forms firstly from the gas–liquid boundary around the bubble, then the hydrate gradually grows up and piles up in the bottom side of the bubble to form a hydrate particle, synchronously. The gas hydrate shape is affected by the gas flow rate, and the hydrate is acicular crystal at the low gas flow rate while the hydrate changes to the fine sand-like crystal at the high gas flow rate. Besides, by the comparison of the CO_2 concentration in the residual gas phase and the amount of the gas consumed in the process of the hydrate formation obtained from the different gas bubble sizes and the different gas flow rates, the effects of the gas bubble sizes and the gas flow rates on the hydrate-based CO_2 capture from IGCC synthesis gas have been achieved systematically. The either small or big gas bubble is proved to be no helpful to the hydrate-based CO_2 separation, and the gas bubble size of 50 μm is ideal in the experiment. When the gas flow rate is lower than 6.75 mL/min/L, the change of the gas flow rate has little effect on the CO_2 separation. However, with the increase of the gas flow rate, the CO_2 concentration in the residual gas phase increases while the gas consumed decreases. The gas flow rate of 6.75 mL/min/L is proved to be a suitable value in the work under the condition of 3.0 MPa and 274.15 K. At the gas flow rate of 6.75 mL/min/L, the CO_2 concentration can be decreased from 40.0 mol% in the feed gas mixture to 8.9 mol% in the residual gas, and the gas consumed of 411.0 L is obtained in the process. However, the detailed hydrate formation time for one small gas bubble moving from the bottom to the top in the reactor is yet not obtained due to the limitation of measurements, and the work is expected to be completed in our next work.

Acknowledgments

This work was supported by National Natural Science Foundation of China (51076155) and Science & Technology Program of Guangdong Province (2009B050600006), which were gratefully acknowledged.

References

[1] Aaron D, Tsouris C. Separation of CO_2 from flue gas: a review. Separ Sci Technol 2005;40(1–3):321–48.
[2] Freund P, Ormerod WG. Progress toward storage of carbon dioxide. Energ Convers Manage 1997;38:S199–204.
[3] Klara SM, Srivastava RD. US DOE integrated collaborative technology development program for CO_2 separation and capture. Environ Prog 2002; 21(4):247–53.
[4] Dijkstra JW, Jansen D. Novel concepts for CO_2 capture. Energy 2004;29(9–10): 1249–57.
[5] Kotowicz J, Chmielniak T, Janusz-Szymanska K. The influence of membrane CO_2 separation on the efficiency of a coal-fired power plant. Energy 2010; 35(2):841–50.
[6] Li XS, Xu CG, Chen ZY, Wu HJ. Tetra-n-butyl ammonium bromide semi-clathrate hydrate process for post-combustion capture of carbon dioxide in the presence of dodecyl trimethyl ammonium chloride. Energy 2010;35(9): 3902–8.
[7] Spencer DF. Methods of selectively separating CO_2 from a multicomponent gaseous stream; 1997. US.
[8] Ballard AL, Sloan ED. The next generation of hydrate prediction I. Hydrate standard states and incorporation of spectroscopy. Fluid Phase Equilibr 2002; 194:371–83.
[9] Lee HJ, Lee JD, Linga P, Englezos P, Kim YS, Lee MS, et al. Gas hydrate formation process for pre-combustion capture of carbon dioxide. Energy 2010;35(6): 2729–33.
[10] Li XS, Xu CG, Chen ZY, Wu HJ. Hydrate-based pre-combustion carbon dioxide capture process in the system with tetra-n-butyl ammonium bromide solution in the presence of cyclopentane. Energy 2011;36(3):1394–402.
[11] Kang SP, Lee H. Recovery of CO_2 from flue gas using gas hydrate: thermodynamic verification through phase equilibrium measurements. Environ Sci Technol 2000;34(20):4397–400.
[12] Zhang LW, Chen GJ, Guo XQ, Sun CY, Yang LY. The partition coefficients of ethane between vapor and hydrate phase for methane plus ethane plus water and methane plus ethane plus THF plus water systems. Fluid Phase Equilibr 2004;225(1–2):141–4.
[13] Zhong Y, Rogers RE. Surfactant effects on gas hydrate formation. Chem Eng Sci 2000;55(19):4175–87.
[14] Lin W, Chen GJ, Sun CY, Guo XQ, Wu ZK, Liang MY, et al. Effect of surfactant on the formation and dissociation kinetic behavior of methane hydrate. Chem Eng Sci 2004;59(21):4449–55.
[15] Li XS, Xia ZM, Chen ZY, Yan KF, Li G, Wu HJ. Equilibrium hydrate formation conditions for the mixtures of $CO_2 + H_2 +$ Tetrabutyl ammonium bromide. J Chem Eng Data 2010;55(6):2180–4.
[16] Li XS, Xu CG, Chen ZY, Cai J. Synergic effect of cyclopentane and tetra-n-butyl ammonium bromide on hydrate-based carbon dioxide separation from fuel gas mixture by measurements of gas uptake and X-ray diffraction patterns. Int J Hydrogen Energ 2012;37(1):720–7.
[17] Vysniauskas A, Bishnoi PR. A kinetic-study of methane hydrate formation. Chem Eng Sci 1983;38(7):1061–72.
[18] Englezos P, Kalogerakis N, Dholabhai PD, Bishnoi PR. Kinetics of gas hydrate formation from mixtures of methane and ethane. Chem Eng Sci 1987;42(11): 2659–66.
[19] Skovborg P, Ng HJ, Rasmussen P, Mohn U. Measurement of induction times for the formation of methane and ethane gas hydrates. Chem Eng Sci 1993;48(3): 445–53.
[20] Fukumoto K, Tobe J, Ohmura R, Mori YH. Hydrate formation using water spraying in a hydrophobic gas: a preliminary study. Aiche J 2001;47(8): 1899–904.
[21] Ohmura R, Kashiwazaki S, Shiota S, Tsuji H, Mori YH. Structure-I and structure-H hydrate formation using water spraying. Energ Fuel 2002;16(5): 1141–7.
[22] Maini BB, Bishnoi PR. Experimental investigation of hydrate formation behavior of a natural-gas bubble in a simulated deep-sea environment. Chem Eng Sci 1981;36(1):183–9.
[23] Englezos P, Kalogerakis N, Dholabhai PD, Bishnoi PR. Kinetics of formation of methane and ethane gas hydrates. Chem Eng Sci 1987;42(11):2647–58.
[24] Sun CY, Chen GJ, Ma CF, Huang Q, Luo H, Li QP. The growth kinetics of hydrate film on the surface of gas bubble suspended in water or aqueous surfactant solution. J Cryst Growth 2007;306(2):491–9.
[25] Luo YT, Zhu JH, Fan SS, Chen GJ. Study on the kinetics of hydrate formation in a bubble column. Chem Eng Sci 2007;62(4):1000–9.
[26] Lekse J, Taylor CE, Ladner EP. Effect of bubble size and density on methane conversion to hydrate. J Petrol Sci Eng 2007;56(1–3):97–100.
[27] Hashemi S, Macchi A, Servio P. Gas-liquid mass transfer in a slurry bubble column operated at gas hydrate forming conditions. Chem Eng Sci 2009; 64(16):3709–16.
[28] Elwell D, Scheel HJ. Crystal growth from high temperature solutions. London: Academic Press; 1975. p. 273.
[29] Sloan ED. Clathrate hydrates of natural gases. In: Koh CA, editor. Chemical industrial series:119. 3rd ed. Golden, Colorado, U.S.A: CRC Press; 2008. p. 721.